ARTICLE NO. 78-993R

J80-168

Computation of a Supersonic Flow Past an Axisymmetric Nozzle Boattail with Jet Exhaust

20007
20019
60001

Ameer G. Mikhail*
University of Dayton, Dayton, Ohio
and
Wilbur L. Hankey† and Joseph S. Shang‡
Air Force Flight Dynamics Laboratory, Wright-Patterson AFB, Ohio

Numerical solutions for supersonic flow at Mach number 1.5 past the AGARD 10 deg axisymmetric nozzle boattail with jet exhaust are obtained using the Navier-Stokes equations. The major objective is to show that such a complex flow can be computed successfully, rather than emphasizing accuracy or computational efficiency. MacCormack's explicit second-order accurate scheme is used together with surface-oriented coordinates obtained through a numerical mapping procedure. Five cases were computed showing the effects of boattail geometry, jet exhaust temperature, boattail temperature, and the differences from the corresponding two-dimensional nozzle geometry. It was found that the hot exhaust and the hot boattail surface both result in lower pressure drag. The surface pressure coefficient distribution and contours of other variables are provided. Comparison with the limited available experimental results is made with the possible interpretation for the deviation being discussed. Several recommendations for improving accuracy are suggested.

I. Introduction

THE aerodynamic characteristics of propulsive elements in aircraft influence the design and performance of the airborne vehicle in an integrated manner. The pressure drag of the jet engine exhaust nozzle, for example, contributes considerably to the total drag of the jet propelled vehicle. Its minimization, therefore, receives considerable attention by experimentalists for optimum boattail design. The pressure drag on the nozzle surface cannot be properly computed without considering the mutual effects of the exhaust jet and the outer stream. Therefore the domain of mutual influence, as seen in Fig. 1, must be studied. Usually the forebody flow region is computed using inviscid theorems, except near the walls where the viscous layer is solved using the thin layer approximation. However, for the afterbody domain near the mixing region, the full Navier-Stokes equations should be used uniformly in that region to capture the viscous interaction.

The nozzle-afterbody problem is usually investigated through wind tunnel testing. Numerical and analytical approaches, however, were investigated by several authors[1-3] using patching procedures for different regions, or other restrictive assumptions such as that of the solid plume simulator. In the present work it is shown that numerical solutions can be obtained for arbitrary nozzle boattails without patching or plume simulators, thus providing good estimates for engine designers. This work was done for the purpose of developing techniques for estimating the aerodynamic properties of aircraft components and also as a forward step for the design integration concept. This work is the second stage of a two-stage project. The completed work of the air intake inlet problem was the first stage.[4]

For the present case, two distinct flow features exist for different nozzle pressure ratios. For low nozzle presure ratios, the weak shock pattern of repeated diamonds occurs. For high nozzle pressure ratios, the strong shock pattern occurs with a Mach disk. The "critical" nozzle static pressure ratio, as discussed in Ref. 5, is different from the familiar value of 1.9-2.2 which is usually encountered for right cylinder nozzle boattails with no external flow. It is expected to be higher for curved boattails with external flow.

To test and verify the numerical computation, experimental results must be available for comparison. Limited experimental results are available for the parallel mixing of two supersonic streams. However, there are numerous results for sonic jets exhausting into static air, mainly for the study of the exhaust plume structure. Also several results are available for a subsonic external stream. In Ref. 6, three AGARD convergent nozzles were tested, but only the boattail surface pressure coefficient results were reported. Results for hot jet exhaust and different Mach numbers were also presented for some of these three geometries. No other results for the flow variables were presented including any information downstream of the nozzle exit station. Reference 7 presented near-exit-plane measurements for the total pressure, temperature, and static temperature. The Mach profiles were then deduced and many results of the exhaust plume static temperature distribution were given for different configurations of nozzles with splitter plates.

The present work objectives are twofold: The first is to demonstrate that such complex flowfields can be numerically computed, providing jet engine designers with information

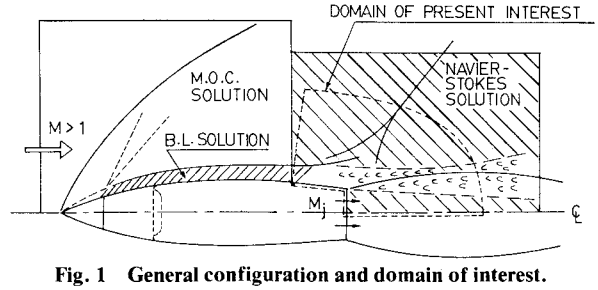

Fig. 1 General configuration and domain of interest.

Presented as Paper 78-993 at the AIAA/SAE 14th Joint Propulsion Conference, Las Vegas, Nev., July 25-27, 1978; submitted Feb. 7, 1979; revision received Jan. 14, 1980.

Index categories: Viscous Nonboundary-Layer Flows; Jets, Wakes, and Viscid-Inviscid Flow Interactions; Airbreathing Propulsion.

*Aerospace Engineer, Research Institute; presently, Dept. of Aerospace Engineering, University of Cincinnati, Ohio. Member AIAA.

†Senior Scientist. Member AIAA.

‡Aerospace Engineer. Member AIAA.

about the estimated drag. This goal is stressed throughout the paper rather than emphasizing accuracy or efficiency of computation. The second is to show that the engine-airframe design integration concept can be applied for this particularly important part of the aircraft.

II. Formulation of Problem

To formulate the problem, the region of computation must first be examined and then the appropriate coordinate system chosen. Next, the best use of the grid points should be made by the appropriate clustering. A surface-oriented coordinate system is adopted where body lines can be aligned along one of the coordinates for treatment of the boundary conditions. This can be achieved as demonstrated in Ref. 8 through numerical mapping. Then the governing equations for turbulent flow, in mass averaged variables,[9] are written in the transformed plane. The boundary conditions are then specified along the proper boundaries. Finally, a simple turbulence model is implemented. Details of the formulation of the problem are presented next.

Region of Computation

First, the AGARD 10 deg nozzle general schematic configuration is shown in Fig. 2. (The exact dimensions can be found in Refs. 5 and 6, the Arnold Engineering Development Center (AEDC) nozzle model is also given in Ref. 5). The domain of computation is depicted in Fig. 2 with an axial length of 40.48 cm, which is about four times the nozzle exit diameter. Only a length of 25.3 cm of the boattail nozzle was considered for computation to reduce the required grid points and computer time. Further, the line normal to the boattail wall at the starting station $x=0$, was taken to be 30.36 cm with the estimate of 2.83 cm for the turbulent boundary layer thickness. Finally, the outer boundary was taken to follow the nozzle boattail contour, as shown in Fig. 2.

Coordinate System

The cylindrical coordinate system (r,θ,x) is used, with the θ dependency being dropped for the axisymmetry formulation. The u,v are the velocity components along the x and r directions, respectively. A coordinate system as that of Fig. 2 was chosen using the approach of Ref. 8 which maps that region into a unit square. The lines parallel to the boattail wall are the $\eta=$const lines, which orthogonally intersect with the axis of symmetry. The lines normal to the boattail wall are the $\zeta=$const lines, with the constant equal to zero at the station $x=0$. These lines are gradually less steep and align themselves along "rays" of the exiting jet and finally coincide with the axis of symmetry, where $\zeta=1.0$. It was found essential for successful computation that the $\eta=$const lines should not sharply turn at the lip of the nozzle boattail and coincide with the vertical "line" representing the actual exit plane. It was essential to have these lines smoothly curve away from the exit plane as shown in Fig. 2. The sharp turn manifests itself in stiff transformation derivatives, causing numerical instability when solving the governing equations. This problem of placing the jet conditions is alleviated if the internal jet flow inside the nozzle is being solved simultaneously with the external flow. More details regarding this observation and the coordinate system can be found in Ref. 5.

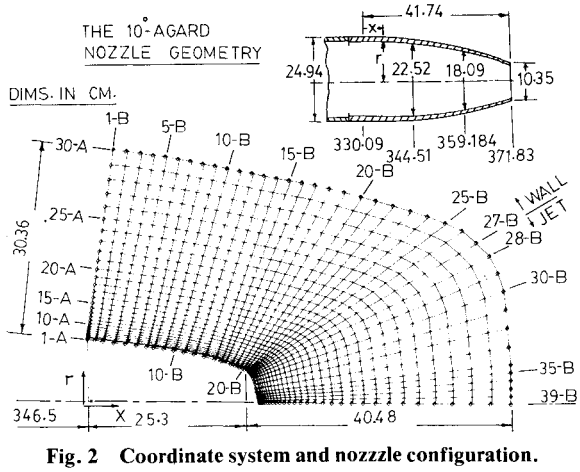

Fig. 2 Coordinate system and nozzzle configuration.

Governing Equations

The Navier-Stokes equations for axisymmetric and two-dimensional turbulent flows can be written in the following familiar form, where the dependent variables u,v,e are mass averaged as described in Ref. 9, where e is the specific total internal energy, and ρ and P are the mean density and pressure, respectively.

$$\frac{\partial U}{\partial t}+\frac{\partial F}{\partial x}+\frac{1}{r^{j_0}}\frac{\partial (r^{j_0}G)}{\partial r}=j_0\cdot\frac{H}{r^{j_0}} \tag{1a}$$

where $j_0=1$ or 0 for axisymmetric and two-dimensional flow, respectively, and

$$U=\begin{bmatrix}\rho\\ \rho u\\ \rho v\\ \rho e\end{bmatrix},\quad F=\begin{bmatrix}\rho u\\ \rho uu-\sigma_{xx}\\ \rho uv-\tau_{xr}\\ \rho ue-\dot{q}_x-\sigma_{xx}u-\tau_{xr}v\end{bmatrix}$$

$$G=\begin{bmatrix}\rho v\\ \rho uv-\tau_{xr}\\ \rho vv-\sigma_{rr}\\ \rho ve+\dot{q}_r-\tau_{xr}u-\sigma_{rr}v\end{bmatrix},\quad H=\begin{bmatrix}0\\ 0\\ -\sigma_+\\ 0\end{bmatrix} \tag{1b}$$

where:

$$\sigma_{xx}=-P-\frac{2}{3}(\mu+\epsilon)\nabla\cdot U+2(\mu+\epsilon)\frac{\partial u}{\partial x}$$

$$\sigma_{rr}=-P-\frac{2}{3}(\mu+\epsilon)\nabla\cdot U+2(\mu+\epsilon)\frac{\partial v}{\partial r}$$

$$\sigma_+=-P-\frac{2}{3}(\mu+\epsilon)\nabla\cdot U+2(\mu+\epsilon)\frac{v}{r}$$

$$\tau_{rx}=\tau_{xr}=(\mu+\epsilon)\left(\frac{\partial u}{\partial r}+\frac{\partial v}{\partial x}\right)$$

$$e=C_vT+\tfrac{1}{2}(u^2+v^2)$$

$$\dot{q}_x=-C_p\left(\frac{\mu}{Pr}+\frac{\epsilon}{Pr_t}\right)\frac{\partial T}{\partial x}$$

$$\dot{q}_r=-C_p\left(\frac{\mu}{Pr}+\frac{\epsilon}{Pr_t}\right)\frac{\partial T}{\partial r}$$

$$\nabla\cdot U=\frac{\partial u}{\partial x}+\frac{\partial v}{\partial r}+j_0\frac{v}{r} \tag{1c}$$

The gas (air) was assumed to be perfect and the hot exhaust was modeled as air, satisfying the equation of state

$$P=\rho RT \tag{2}$$

and the coefficient of viscosity was assumed to vary with temperature according to Sutherland's relation

$$\mu = (35.85 \times 10^{-8})\, T^{1.5}/(T + 198.6)\,\mathrm{kg_f - s/m^2} \tag{3}$$

The laminar and turbulent Prandtl numbers, Pr and Pr_t, were assumed constant and of values of 0.72 and 0.9, respectively. Although μ is usually very small compared to ϵ, the effect of temperature gradients in the present problem can be very large, causing large gradients in μ. And because the coefficient of heat conductivity exhibits similar variation with the temperature, it is appropriate to assume that their ratio is almost invariant. The ratio of specific heats γ was also taken as a constant, with a value of 1.4. Finally, the second coefficient of viscosity was not chosen to satisfy the Stokes' hypothesis at the early stage of computations, but rather the relation

$$\lambda = -2/3\,(\mu + \epsilon)\cdot\beta \tag{4}$$

where β is a constant ≤ 1.0 and, usually taken negative to increase the bulk viscosity that acts as numerical damping across shocks.[10] However, β was set equal to 1.0 when a converged solution seemed to be obtained.

In the η-ξ computational plane, Eq. (1a) is transformed to the form:

$$\frac{\partial U}{\partial t} + \left[\xi_x \frac{\partial F}{\partial \xi} + \frac{1}{r^{j_0}}\xi_r \frac{\partial (r^{j_0} G)}{\partial \xi}\right] + \left[\eta_x \frac{\partial F}{\partial \eta} + \frac{1}{r^{j_0}}\eta_r \frac{\partial (r^{j_0} G)}{\partial \eta}\right] = j_0 \cdot \frac{H}{r^{j_0}} \tag{5}$$

where now η and ξ can be considered as the independent variables and ξ_x, ξ_r, η_x, and η_r are the four transformation coefficients obtained numerically from the mapping procedure.

Turbulence Models

The experimental tests[6] for the nozzle geometry under consideration were run at a Reynolds number of 8.2×10^4/cm. Therefore the flow is expected to be fully turbulent with a Reynolds number in excess of 25.0×10^6 at the end of the long cylindrical forebody, at the station 330 cm downstream of the nose tip. This station also marks the beginning of the nozzle boattail and is 16.42 cm upstream of the station where computations began.

Complicated eddy viscosity models can be found in the literature for many flow patterns including the axisymmetric wake problem. It has not yet been demonstrated that use of sophisticated or high-order closure models would necessarily yield better results in general. Many models for the free shear layers, jets, and wakes using the turbulent kinetic energy and other concepts can be found, e.g., in Refs. 12 and 13. It was decided, therefore, to use the simplest model in the mixing region. The eddy viscosity model in the computational domain was split into two or more different models in different regions, as will be explained next.

The computational domain is split into three regions as shown in inset A of Fig. 3. In region I, the simple two-layer algebraic model of Ref. 14 for flat plate is used here since the effect of axisymmetry was estimated to be minor at this flow condition, for a cylinder with a diameter of approximately 10 cm. The inner region for that model is formulated as:

$$\epsilon_i = \rho\left\{0.4 r_n \left(1 - \exp\left[-\frac{r_n\sqrt{\tau_w}}{26\mu}\right]\right)\right\}^2 \cdot \left|\frac{\partial u_t}{\partial r_n}\right| \tag{6a}$$

and the outer region model is formulated as:

$$\epsilon_0 = 0.0168 \rho u_e \delta^*_{\mathrm{inc}} \tag{6b}$$

where r_n is the normal distance measured from the boattail wall, τ_w the wall shear stress, u_t the tangential velocity in a direction parallel to the wall, u_e the average tangential velocity outside the boundary layer of the velocity profile at that station, here taken as u_t at the point of index $j = 15$ (approximately $r_n \simeq 5$ cm), and

$$\delta^*_{\mathrm{inc}} = \int_0^{\delta} \left(1 - \frac{u_t}{u_e}\right) \mathrm{d}r_n$$

In region III, the eddy viscosity model for a jet is used. It increases in the axial direction while remaining constant in planes normal to the axis of symmetry. The following model was used:

$$\epsilon_{\mathrm{III}} = \epsilon_{\mathrm{in}}(1 + S) \tag{7}$$

where S is the dimensionless distance along the "rays" of the coordinates $\xi = \mathrm{const}$, measured from the jet exiting station, and ϵ_{in} is the initial value at the jet exiting station. In region II, linear variation (with respect to the indexing parameter i) for the values between the last "ray" in region I and the first ray of region III was used. This was done to avoid sudden changes in the ϵ values, and also to cover the region of possible flow separation, where the proper turbulence model still needs to be investigated.

The second composite model of sketch B of Fig. 3 was also used but its results are not presented here. No major differences were observed in the results using these two models. In this case, region III of sketch A is split further into two separate regions, III and IV. In the new region III, a model similar to that of Ref. 15 is used with minor modifications. In the present study, the model used was:

$$\epsilon_{\mathrm{III}} = \frac{1}{RT}\frac{b}{\alpha}\left|(u_{i,j} - u_{\ell,j})\right|$$

where b is the "width" of the mixing region as shown in Fig. 3, RT the turbulence Reynolds number, taken as $[330.0 - 333.0\, e^{-(0.495 M_{i,j})}]$, $u_{\ell,j}$ the u velocity at the center line and α a factor for axisymmetry effects.

The value of 3.0 was used for α in the present case. Finally, the value of ϵ in region IV was set to zero, representing the inviscid core region. The value of ϵ in region II was also taken as the linear interpolation between the values of regions I and III as described previously.

In the computation, the nondimensional y^+ for the first point away from the wall was assumed to be large ($\simeq 70$) to allow for a larger time step. This value should be about 10 if the skin friction coefficient is to be computed with fair accuracy. In the present work the surface pressure distribution, which is less sensitive to the spatial step size normal to the wall, was the primary concern.

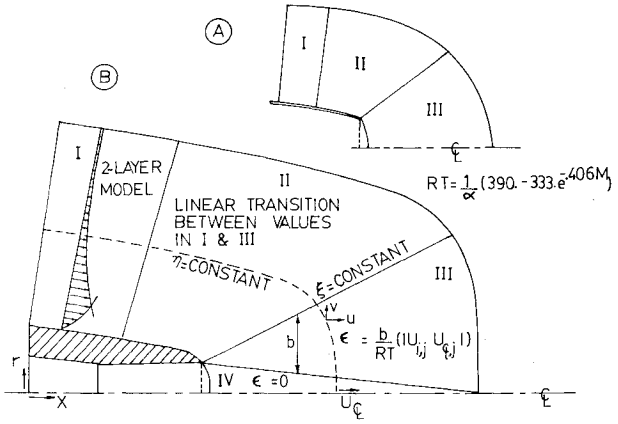

Fig. 3 Eddy viscosity model.

Boundary Conditions

Incoming Flow Conditions at Station $x=0$ ($\xi=0.0$)

The Mach number and all flow variables are not known at this station and therefore some engineering judgment was required, bearing in mind the major objective of the present work. Of course, a solution to the full flowfield starting at the upstream undisturbed condition would omit the necessity for such judgments. First, it is assumed that the Mach number is still 1.5 at the end of the cylindrical forebody at station 330 cm, i.e., that the compression effect at the nose tip is equally offset by the expansion at the forebody shoulder (see Ref. 6 for details of the test model configuration). Moreover, since computations for the curved boattail start at the station 16.42 cm downstream from station 330.1, the use of the value $M=1.5$ is not representative of the real flow case. In fact, the tangential Mach number at the station $x=0$ was taken as 1.74 based upon a Prandtl-Meyer expansion for a 7 deg turning angle. Both the u and v velocity components were than computed. The turbulent profile for the tangential velocity was assumed to be of the (1/7) power profile, with the boundary-layer thickness estimated as 2.83 cm. The static temperature and pressure profiles were assumed uniform along that line, with values of $0.905T_{\infty e}$ and $0.7P_{\infty e}$, respectively, corresponding to the 7 deg expansion turn. The density, specific internal energy, and the eddy viscosity profiles were then computed and imposed as the boundary values.

Conditions on Symmetry Line $r=0$ ($\xi=1.0$)

Because of symmetry, the derivative in the direction normal to the centerline was taken to be zero for certain variables. Since not all of the variables should be extrapolated in this manner (otherwise inconsistency and overspecification would result), the following sequence was followed: 1) $\partial(\rho e)/\partial\xi$, $\partial\rho/\partial\xi$, $\partial u/\partial\xi$, $\partial\epsilon/\partial\xi$, and v were set to zero; 2) P was computed from the equation of state using ρ and e; and 3) ρu and ρv were computed.

Conditions on Farfield Boundary ($\eta=1.0$)

The variation along the $\xi=$ constant lines was assumed to vanish, therefore the following conditions were applied: 1) $\partial u/\partial\eta$, $\partial v/\partial\eta$, $\partial(\rho e)/\partial\eta$, $\partial\rho/\partial\eta$, and $\partial\epsilon/\partial\eta$ were set to zero; 2) P was computed from the equation of state using ρ and e; and 3) ρu and ρv were computed.

Conditions on Wall and at Jet Exit ($\eta=0.0$)

On the boattail wall: 1) u and v are zero for no slip, then ρu, ρv, and also ϵ are zero. T is set as T_w, taken equal to T_{0e} or otherwise specified for hot wall cases; 2) $\partial P/\partial\eta$ is set to zero; 3) ρ is computed from the equation of state, utilizing P and T; and 4) ρe is computed from ρ, u, v, and T.

For the jet exit plane: 1) uniform profiles $u=u_j$, $T=T_j$, $P=P_j$, and $v=0$, where u_j, T_j, and P_j are computed from given T_{0j}, P_{0j}, and R_{ej}; 2) assuming an exit Mach number of 1.01, ρ is computed from the equation of state and ϵ computed as $(100\,\mu)$; and 3) ρu, ρv, and ρe are computed.

The u velocity at the first grid point in the jet flow nearest to the inner nozzle surface was set to 0.5 u_j to reflect the effects of viscosity and simulate the corresponding boundary layer.

III. Numerical Method

The time-dependent, predictor-corrector MacCormack's explicit scheme[16-18] is used to solve Eq. (5) in two steps in the η and ξ directions. For the present case, the dependent vector variable $U(\eta,\xi,t)$ was advanced in time as:

$$U(\eta,\xi,t+\Delta t)=[L_\xi^{M/2}(\Delta t_\xi/2)L_\eta(M\Delta t_\xi)L_\xi^{M/2}\times(\Delta t_\xi/2)]\cdot U(\eta,\xi,t)$$

with

$$\Delta t=M\Delta t_\xi, \quad \text{if} \quad \Delta t_\xi<\Delta t_\eta \tag{8a}$$

or as

$$U(\eta,\xi,t+\Delta t)=[L_\eta^{N/2}(\Delta t_\eta/2)L_\xi(N\Delta t_\eta)L_\eta^{N/2}\times(\Delta t_\eta/2)]\cdot U(\eta,\xi,t)$$

with

$$\Delta t=N\Delta t_\eta, \quad \text{if} \quad \Delta t_\eta<\Delta t_\xi \tag{8b}$$

where M and N are the smallest even integers of $\Delta t_\eta/\Delta t_\xi$ and $\Delta t_\xi/\Delta t_\eta$, respectively, and Δt_η, Δt_ξ are the maximum allowable time steps in the η and ξ directions as determined by the Courant-Friedrichs-Lewy (CFL) limit with viscous stability requirement as given by Eq. (9). The values of M and/or N were chosen to be 2 for the present work. This particular procedure was necessary for the present case because, depending upon the relative flow conditions of the external flow to the jet flow, $(\Delta t_\eta/\Delta t_\xi)$ can change drastically from less than to greater than 1.0. This procedure was automated in the computer program. Also, this frequent change of the solution path (M or $N=2$) was intended for the present coordinate system for proper and frequent forcing of the boundary conditions.

The maximum time step allowed was estimated as:

$$\Delta t=\min_{i,j}(\Delta t_\eta,\ \Delta t_\xi)=\min_{i,j}\left[\left.\frac{\Delta S_\eta}{|u_\eta|+C}\right|_{i,j},\ \left.\frac{\Delta S_\xi}{|u_\xi|+C}\right|_{i,j},\right.$$

$$\Delta S_\eta/\max\left\{\frac{2\gamma}{\rho}\left(\frac{\mu}{Pr}+\frac{\epsilon}{Pr_t}\right)\frac{1}{\Delta S_\eta},\ \frac{\sqrt{-\lambda_t(\mu+\epsilon)}}{\Delta S_\xi}\right\},$$

$$\left.\Delta S_\xi/\max\left\{\frac{2\gamma}{\rho}\left(\frac{\mu}{Pr}+\frac{\epsilon}{Pr_t}\right)\frac{1}{\Delta S_\xi},\ \frac{\sqrt{-\lambda_t(\mu+\epsilon)}}{\Delta S_\eta}\right\}\right] \tag{9}$$

where u_η, ΔS_η and u_ξ, ΔS_ξ are the velocity and mesh side lengths in the η and ξ directions, respectively. The actual time step used was usually less than this estimated maximum. A factor of 0.7 was used.

Numerical Damping

The fourth-order pressure gradient "damping" as introduced by MacCormack and Baldwin[17] is used here. This is implemented by replacing

$$F_{ii,j} \quad \text{by} \quad F_{ii,j}+F_{Dii,j} \tag{10a}$$

and

$$G_{ii,j} \quad \text{by} \quad G_{ii,j}+G_{Dii,j} \tag{10b}$$

in both the predictor and corrector steps of the ξ solution sweep for Eq. (5), with $ii=i$ and $(i+1)$ for the predictor and corrector steps, respectively. The following expressions for F_D and G_D were used

$$F_{Dii,j}=C_{\xi_1}(|u_{ii,j}|+C_{ii,j})\frac{|P_{i+1,j}-2P_{i,j}+P_{i-1,j}|}{(P_{i+1,j}+2P_{i,j}+P_{i-1,j})}$$

$$G_{Dii,j}=C_{\eta_1}(|v_{ii,j}|+C_{ii,j})\frac{|P_{ii,j+1}-2P_{ii,j}+P_{ii,j-1}|}{(P_{ii,j+1}+2P_{ii,j}+P_{ii,j-1})}$$

where

$$C_{\xi_1}=0.02\xi^2_{x_{ii,j}}+0.12\xi^2_{r_{ii,j}} \qquad C_{\eta_1}=0.01\eta^2_{r_{ii,j}}+0.09\eta^2_{x_{ii,j}}$$

The constants in the last two expressions were chosen after some numerical experimentation. They should be changed for different flow conditions. Similar expressions are used during the η sweep solution, which can be found in Ref. 5.

The normal stress damping, represented by the factor β in Eq. (4), was described in the formulation of the problem. The value of $\beta = -6$ was used here.

Finally, although MacCormack's scheme is second-order accurate, the use of a two-point, first-order accurate formula for the boundary conditions, as applied here and by most investigators, reduces the overall accuracy. However, it has also been experienced that the use of three-point, second-order forms for boundary conditions may sometimes lead to numerical instability.

IV. Results and Discussion

A total of five different cases were computed. Four cases were computed for the specific nozzle boattail under consideration (the AGARD 10-deg nozzle) and one case for a similar AEDC model with cold exhaust to study the effects of the nozzle boattail geometry.

The experimental results[6] of the base case of the cold exhaust were obtained under the following test conditions for the external flow: $M_{\infty_e} = 1.5$, $T_{0e} = 580°\text{R}$, $Re_e = 8.2 \times 10^4/\text{cm}$ with the jet exhaust being under the conditions $T_{0j} = 540°\text{R}$, throat Reynolds number $= 1.773 \times 10^6$, and the nozzle exit diameter $= 10.07$ cm. (Subscripts ∞, 0; e, j refer to the freestream and total conditions; the external and jet stream, respectively.) These conditions will yield a nozzle pressure ratio (NPR) of 7.09, where NPR is defined here as P_{0j}/P_{∞_e}. The ratio P_j/P_{∞_e} is only 3.746.

The hot exhaust case computed here was computed with $T_{0j} = 2100°\text{R}$ and the hot boattail wall was computed for $T_w = 1100°\text{R}$. The corresponding two-dimensional case and the AEDC early model case were computed for cold exhaust temperature as in the base case.

All the computations were run on the CDC 6600 computer with a mesh of 30×39 points in the η-ξ plane with $\Delta\eta = 0.344$ and $\Delta\xi = 0.0263$.

Computations were allowed to continue until the accumulative physical time reached at least $4t_{ch}$ where $t_{ch} = L/U_{\infty_e} = 12.9 \times 10^{-4}$ s, where L is the length of the computational region, here 65.78 cm. The convergence criterion was based upon the condition that the maximum change in the static pressure over one t_{ch} should be less than 5%. The largest changes observed were in the static pressure, and particularly along the centerline $r = 0$. For the base case of cold exhaust the maximum change in the pressure along the centerline was 4.5% along the time interval $t = 4.0t_{ch}$ to $t = 5.9t_{ch}$. The computation for this particular case was therefore stopped after $t = 5.9t_{ch}$. For other cases computations were stopped after about $t = 4.0t_{ch}$. This was achieved by making use of the computed case of cold exhaust as the starting initial condition for the rest of the cases, thus eliminating most of the numerical difficulties and achieving faster convergence rates.

The computer time for the typical base case was 0.0022 s/grid point per cycle per one Δt. Cycle here denotes three sweeps, two in the η direction and one in the ξ direction. This amounts to a lot of computer time and it is mainly due to the very small allowable time step for the explicit scheme. For the base case this maximum time step was 0.26×10^{-6} s.

The first set of results obtained, shown in Fig. 4, presents the surface pressure coefficient C_p, where C_p is $(P_w - P_\infty)/(\frac{1}{2}\rho_\infty U_\infty^2)$. In Fig. 4a, results for the base case of cold exhaust are compared with the experimental results of Ref. 6. Although the recompression seems to be weaker than those measured, the deviation between the upper and lower surface measurements is obviously due to the effect of the model support, representing the three-dimensionality of the experimental results, while the computation models true axisymmetry. Also, it can be seen that the smaller C_p com-

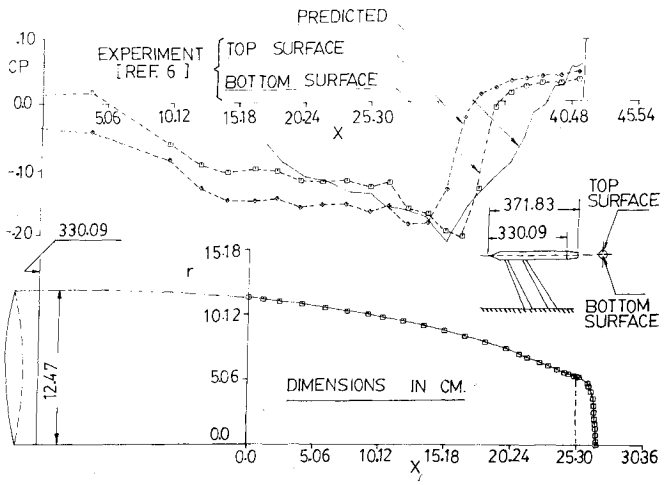

a) Comparison with experiment.

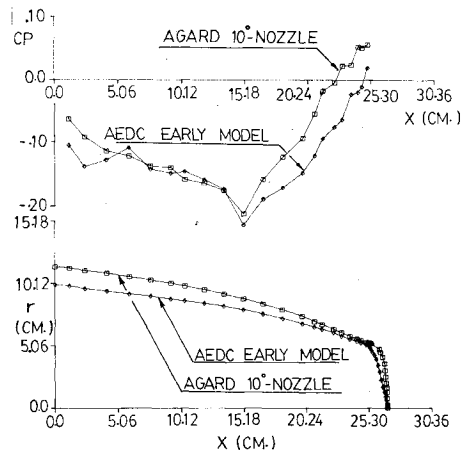

b) Influence of boattail geometry on pressure coefficient distribution.

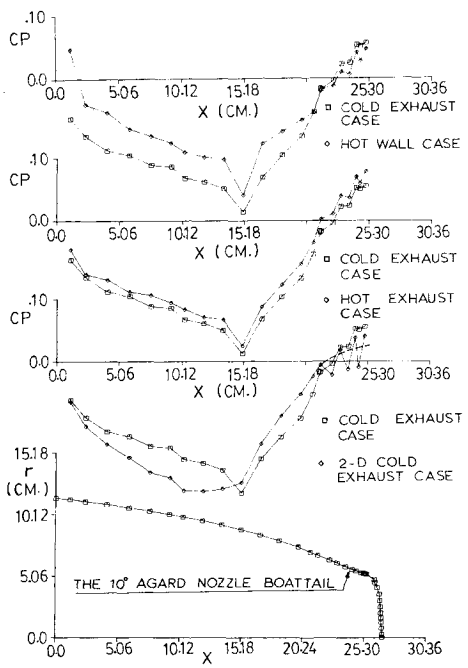

c) Hot wall, hot exhaust, and two-dimensional cases.

Fig. 4 Pressure coefficient distribution.

puted near $x = 0$ is mainly due to the imposed pressure profile.

Although the pressure plateau of the experimental results near the nozzle lip may suggest flow separation, it was reported[6] firmly that no separation was observed during the experiment. The present solution did not show a pressure plateau. In the cases considered, no flow separation was detected.

In Fig. 4b, the effect of change in the boattail geometry to the AEDC geometry is shown by the resulting C_p distribution. Although the C_p is smaller, the nozzle wetted area is larger, resulting in almost equal pressure drag force. But because the AGARD model allows larger engine space, it indicates a better boattail design. The "kink" observed at $x \simeq 5.5$ for the AEDC model lacks reasonable explanation. Figure 4c shows the effects of exhaust temperature, boattail wall temperature, and two-dimensional axisymmetry. The hot exhaust case yielded a smaller pressure drag, 79% of the corresponding drag for the cold exhaust case. The hot boattail surface case yielded a smaller pressure drag, 67% of the same corresponding cold wall case. It is of interest to notice that the effect of the hot exhaust traveled upstream through the subsonic region through the boundary layer.

The two-dimensional result of Fig. 4c showed bad oscillatory behavior for the pressure near $x \simeq 25$. Although disturbances and interaction effects are expected to be larger for the two-dimensional than for the axisymmetric case, this behavior may be partially smoothed if more points are used in that region. A dashed line is drawn to show the expected behavior.

Mach line contours for two cases are given in Fig. 5. It is interesting to see how the subsonic region protrudes after the exit station. Differences in the pattern are observed between the axisymmetric and two-dimensional cases in Fig. 5, where the subsonic region protrudes further in the two-dimensional case.

The static temperature fields, necessary for infrared signature analysis and detection, are given for two cases in Fig. 6. The temperature field downstream of the nozzle exit plane was not affected by the increase of boattail wall temperature. The wall temperature effect was almost confined to the wall region. Finally, the velocity flowfield is given by the arrows in Fig. 7 for the hot wall case. For more clarity, the corresponding stream function was computed and the stream lines were also plotted. No separated flow regions were detected in the different cases computed.

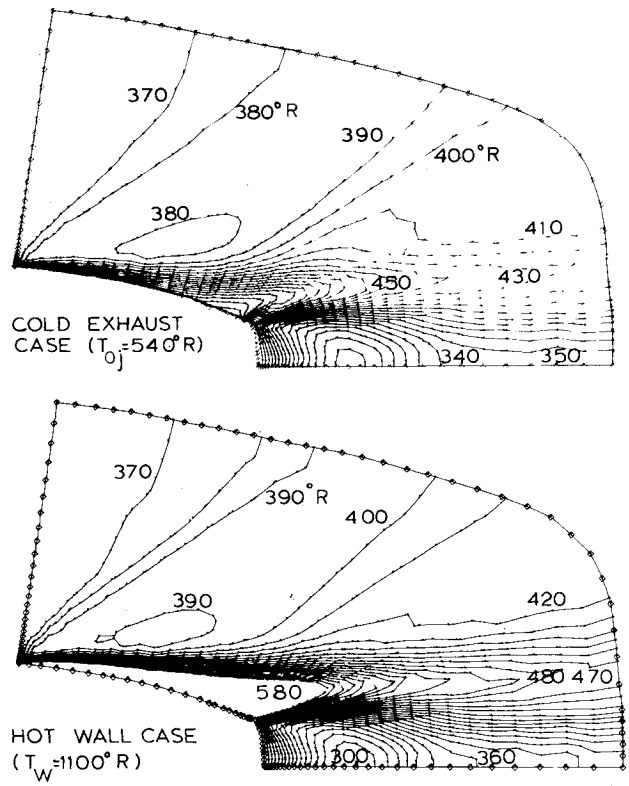

Fig. 6 Static temperature contours.

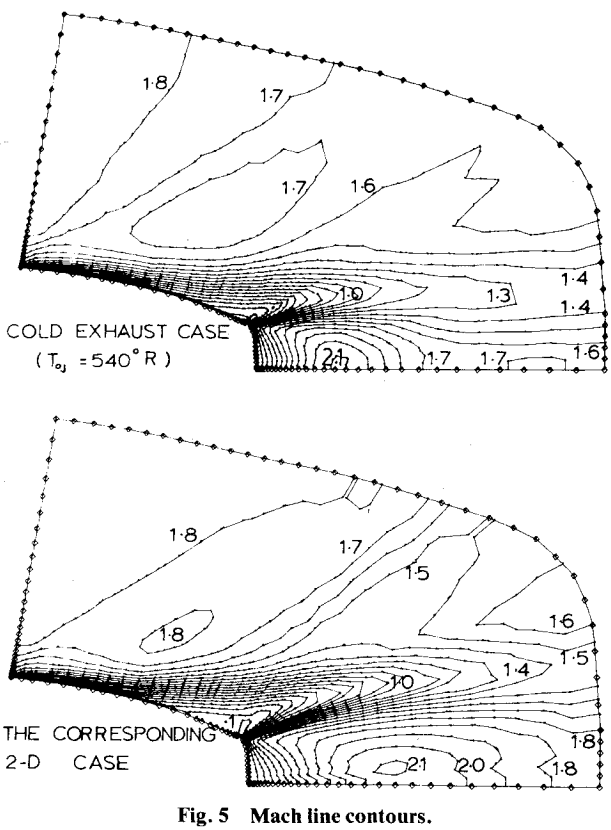

Fig. 5 Mach line contours.

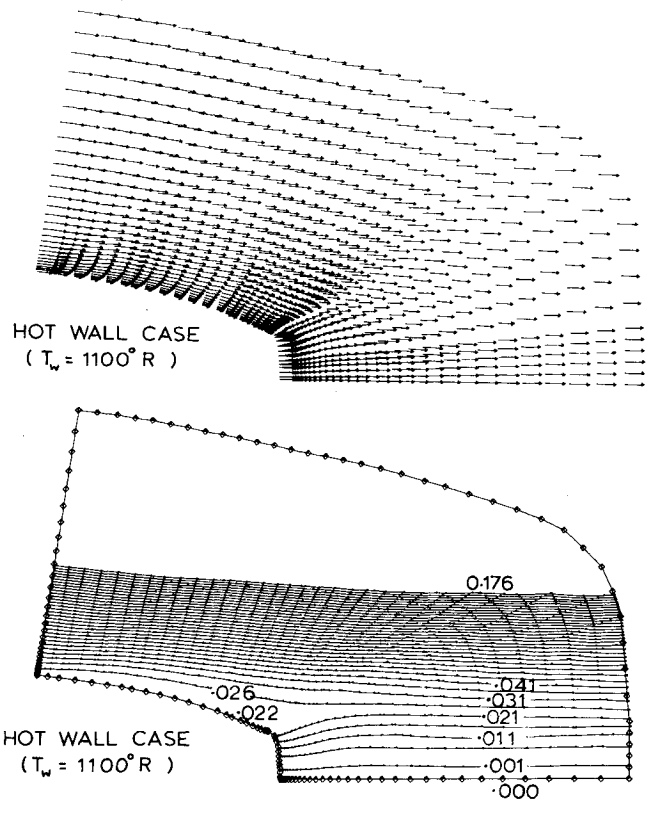

Fig. 7 Velocity flowfield.

It is of interest to observe the decay of the high-pressure and temperature conditions along the axis of the jet. It was found that mixing of the two streams takes place to a point far downstream of the present region limits of about $4D$, where D is the nozzle exit diameter. Other observations regarding the mixing of the external and the jet streams can be found in Ref. 5.

V. Conclusions and Recommendations

Numerical solutions for supersonic flow at a Mach number 1.5, with jet exhaust past the AGARD 10-deg axisymmetric nozzle were obtained using the Navier-Stokes equations in conservative variables. Five different cases were computed showing effects of the nozzle boattail geometry, exhaust temperature, boattail wall temperature, and the differences between the axisymmetric and the corresponding two-dimensional case. The surface pressure distribution was obtained together with details of the flowfield. For the cases studied, the pressure drag was reduced to 67 and 79% for the boattail hot wall and hot exhaust cases, respectively, of the cold wall, cold exhaust reference case.

Computations were made using several engineering assumptions and with few grid points, but still yielded reasonable results. The success of the present work should encourage engine designers to rely on computation as a parallel means to wind tunnel testing.

Several improvements are recommended concerning numerical accuracy and computational efficiency. Regarding accuracy, more grid points and computer time will be needed, especially near the wall if the skin friction coefficient is to be computed with reasonable accuracy. In addition, smoother transformation derivatives are recommended. Further, use of the conservative form of the equations in the transformed plane as suggested by Viviand[11] is favored. Regarding computational efficiency, implicit schemes[19-21] are encouraged to alleviate the small time increment of the explicit scheme necessary for stability.

Further studies should be performed regarding the conditions that facilitate computation for capturing of the strong shock made for the present flow case. A high nozzle pressure ratio case of 15.86, which was shown[6] to have the Mach disk, was tried during the present investigation, but the solution converged only to the weak shock mode since inadequate expansion was obtained. Factors influencing this tendency in computation are now being studied, with some studies regarding this case being available in the literature.[22,23] In addition, studies regarding better turbulence modeling for the present flow case are encouraged for future applications.

Acknowledgments

This work was done while the first author was on a visiting scientist program at the Flight Dynamics Laboratory of Wright-Patterson Air Force Base in Dayton, Ohio. It was fully funded by the U.S. Air Force through Contract F33615-76-C-3145.

References

[1]Holst, T. L., "Numerical Solution of Axisymmetric Boattail Fields with Plume Simulators," AIAA Paper 72-224, Jan. 1977.

[2]Cosner, R. R. and Bower, W. W., "A Patched Solution of the Transonic Flow Field About an Axisymmetric Boattail," AIAA Paper 77-227, Jan. 1977.

[3]Yaros, S. F., "Prediction of Pressure Distributions on Axisymmetric Bodies in Transonic Flow," AIAA Paper 77-226, Jan. 1977.

[4]Knight, D. D., "Numerical Simulation of High Speed Inlets Using the Navier-Stokes Equations," *AIAA Journal*, Vol. 15, Nov. 1977, pp. 1583-1589.

[5]Mikhail, A. G., "Numerical Solution of a Supersonic Nozzle Afterbody Flow with Jet Exhaust," Univ. of Dayton Rept. UDR-TR-79-43, Dec. 1978; also AFFDL Tech. Rept.

[6]Galigher, L. L., Yaros, S. F., and Bauer, R. C., "Evaluation of Boattail Geometry and Exhaust Plume Temperature Effects on Nozzle Afterbody Drag at Transonic Mach Numbers," Arnold Engineering Development Center, AEDC-TR-76-102, Oct. 1976.

[7]Segalman, I. and Semarjian, H., "Turbine Engine Infrared Signature Program—Final Report," Air Force Aero Propulsion Laboratory, Dayton, Ohio, AFAPL-TR-76-38, June 1976.

[8]Thompson, J. F., Thames, J. C., and Mastin, W. C., "Automatic Numerical Generation of Body-Fitted Curvillinear Coordinate System for Field Containing any Number of Arbitrary Two-Dimensional Bodies," *Journal of Computational Physics*, Vol. 15, 1974, pp. 299-319.

[9]Rubesin, M. W. and Rose, W. C., "The Turbulent Mean-Flow Reynolds Stress and Heat-Flux Equations in Mass-Averaged Dependent Variables," NASA TM X-62.248, March 1973.

[10]McRae, D. S., "The Conically Symmetric Navier-Stokes Equations: Numerical Solution for Hypersonic Cone Flow at High Angle of Attack," AFFDL-TR-76-139, March 1977.

[11]Viviand, H., "Conservation Forms of Gas Dynamics Equations," *La Recherche Aerospatiale*, Jan.-Feb. 1974, pp. 65-66.

[12]*Free Turbulent Shear Flows, Vol. I—Conference Proceedings*, Proceedings of a conference held at Langley Research Center, July 20-21, 1972; published as NASA-SP-321, 1973.

[13]*Symposium on Turbulent Shear Flows*, April 18-20, 1977, Penn. State Univ., University Park, Pa.

[14]Cebeci, T., Smith, A.M.O., and Mosinskis, G., "Calculations of Compressible Adiabatic Turbulent Boundary Layers," *AIAA Journal*, Vol. 8, Nov. 1970, pp. 974-982.

[15]Peters, C. E. and Phares, W. J., "Analytical Model of Supersonic, Turbulent Near-Wake Flows," AEDC-TR-76-127, Arnold Engineering Development Center, Sept. 1976.

[16]MacCormack, R. W., "Numerical Solution of the Interaction of a Shock Wave with a Laminar Boundary Layer," *Lecture Notes in Physics*, Vol. 8, Springer-Verlag, New York, 1971, pp. 151-163.

[17]MacCormack, R. W. and Baldwin, B. S., "A Numerical Method for Solving the Navier-Stokes Equations with Applications to Shock-Boundary Layer Interactions," AIAA Paper 75-1, Jan. 1975.

[18]MacCormack, R. W. and Paullay, A. G., "Computational Efficiency Achieved by Time Splitting of Finite Difference Operators," AIAA Paper 72-154, Jan. 1972.

[19]Shang, J. S. "A Hybrid Implicit-Explicit Numerical Technique for Solving the Navier-Stokes Equations," AIAA Paper 77-646, June 1977.

[20]Beam, R. M. and Warming, R. F., "An Implicit Factored Scheme for the Compressible Navier-Stokes Equations," AIAA Paper 77-645, June 1977.

[21]Hung, C. M. and MacCormack, R. M., "Numerical Solution of Supersonic Laminar Flow Over a Three-Dimensional Compression Corner," AIAA Paper 77-694, June 1977.

[22]Auld, D. J. and Bird, G. A., "Monte Carlo Simulation of Regular and Mach Reflection," *AIAA Journal*, Vol. 15, June 1977, pp. 638-641.

[23]Griffin, M. D. and Anderson, J. D., "On the Application of Boundary Conditions to Time Dependent Computations for Quasi One-Dimensional Fluid Flows," *Computers and Fluids*, Vol. 5, 1977, pp. 127-137.